

Higher Harmonic Atomic Force Microscopy: Imaging of Biological Membranes in Liquid

Johannes Preiner, Jilin Tang, Vasilli Pastushenko, and Peter Hinterdorfer*

Institute for Biophysics, Johannes Kepler University of Linz, A-4040 Linz, Austria

(Received 3 May 2007; published 25 July 2007)

The contribution of higher harmonics to the movement of a dynamic force microscope cantilever interacting with a sample in liquid was investigated. The amplitude of the second harmonic has been found to be an order of magnitude higher in liquid than in air, reflecting an increased sensitivity to local variations in elasticity and interaction geometries. A theoretical model of the tip-sample interactions in liquid was introduced and shown to be consistent with experimental findings. Second harmonic amplitude images were recorded on soft biological samples yielding a lateral resolution of ~ 0.5 nm.

DOI: [10.1103/PhysRevLett.99.046102](https://doi.org/10.1103/PhysRevLett.99.046102)

PACS numbers: 68.37.Ps, 07.79.Lh, 62.25.+g, 87.16.Dg

Since its invention in 1986, the Atomic Force Microscope (AFM) [1] has been widely used for the investigation of soft matter and biological samples. Dynamic AFM modes (MAC mode [2], tapping mode [3,4]) have been found to be more gentle compared to contact mode AFM, since the lateral forces acting on the sample during scanning are dramatically reduced [5]. With these techniques, material properties using the phase [6–8] or anharmonic contributions [9] of the cantilever movement when interacting with a sample in air or vacuum can be achieved.

In this Letter, we investigate the motion of a cantilever interacting with a sample under highly over-damped conditions in liquids. The nonlinearity of the interaction forces gives rise to complex dynamics in the tip motion, which can be utilized to obtain information about the elastic properties of the sample. We show that for low quality (Q)-factors of the cantilever oscillation, higher harmonics (i.e., integer multiples of the excitation frequency) significantly contribute to the motion. A simple point mass model was introduced, to qualitatively explain the origin of these contributions and compared to experimental findings. Furthermore, the second harmonic amplitude was recorded during scanning a bacterial surface (S)-layer and a layer of human rhinovirus serotype 2 (HRV2) revealing a lateral resolution of ~ 0.5 nm under physiological conditions.

The equation of motion of a cantilever tip immersed in liquid can be approximated by a one-dimensional forced harmonic oscillator with damping, yielding the nonlinear, second order differential equation [10]

$$m\ddot{x} + \frac{m\omega_0}{Q}\dot{x} + kx = F_0 \cos(\omega t) + F_{\text{hyd}}(d_{\text{ts}}) + F_{\text{ts}}(d_{\text{ts}}). \quad (1)$$

Here, $x(t)$ is the transverse displacement of the cantilever at time t ; m , Q , ω_0 , and k are the mass, the quality factor, angular resonance frequency, and force constant of the free cantilever, respectively. On the right of Eq. (1), F_0 and ω are the amplitude and the angular frequency of the (magnetic) driving force, respectively. $F_{\text{hyd}}(d_{\text{ts}})$ is the additional hydrodynamic force acting on the cantilever when oscil-

lating at a separation d_{ts} to a surface in liquid. The origin of this force is the liquid, which is squeezed out between the cantilever beam and the surface [11]. $F_{\text{hyd}}(d_{\text{ts}})$ varies significantly only at separations d_{ts} comparable to the length scale of the cantilever (~ 100 μm), but it is essentially constant at separations where the nonlinear tip-surface interactions $F_{\text{ts}}(d_{\text{ts}})$ dominate the dynamic behavior of the cantilever. F_{ts} is the sum of an attractive van der Waals force and the repulsive force due to elastic interactions between the tip and the surface [10]. Alternatively, other models could be used to account for the attractive interaction, but would lead to qualitatively similar dynamics [12]. Since in our experiments physiological salt concentrations were used (150 mM PBS), the Debye length is short enough for the electrostatic double layer force to be neglected. The attractive van der Waals force for a sphere-flat geometry is

$$F_{vdW}(d_{\text{ts}}) = -\frac{HR}{6d_{\text{ts}}^2} \quad \text{for } d_{\text{ts}} \geq a_0, \quad (2)$$

where H , R , and a_0 are the Hamaker constant, the tip radius, and an intermolecular distance which is usually introduced to avoid unphysical divergence of F_{ts} [13], respectively. The elastic interaction of the tip in contact with the surface can be described in the framework of the Derjaguin-Muller-Toporov (DMT) [14] contact mechanics, yielding

$$F_{\text{DMT}}(d_{\text{ts}}) = -\frac{HR}{6a_0^2} + \frac{4}{3}E^*\sqrt{R}(a_0 - d_{\text{ts}})^{3/2} \quad \text{for } d_{\text{ts}} < a_0, \quad (3)$$

E^* being the combined Young modulus of the tip and the surface and the first term accounting for the adhesion force. Amplitude vs. distance curves were simulated by numerically solving the equation of motion, Eq. (1) at discrete distances (step size 0.1 nm) between the tip rest position $d = d_{\text{ts}}(t) - x(t)$ and the surface. The integration was performed using a fourth order Runge-Kutta algorithm [15]. At each step, the frequency spectra was calculated from the solution $x(t)$ using a Fast Fourier Transform (FFT) analysis

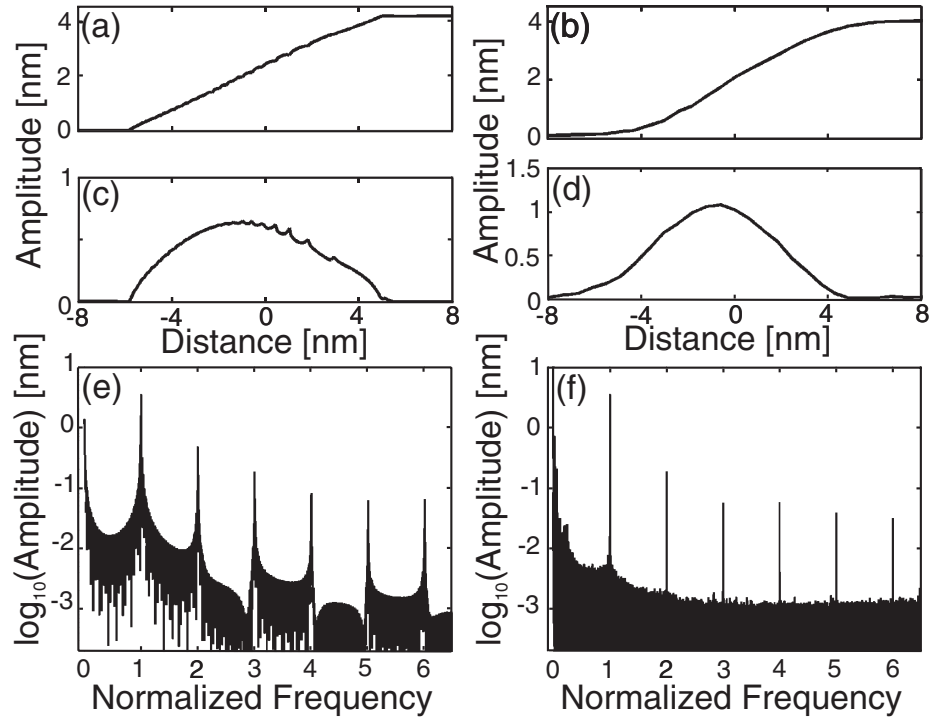


FIG. 1. Comparison between simulation and experimental data obtained for a silicon nitride tip interacting with a mica surface in buffer solution. (a) Simulated amplitude vs. distance curve. (b) Measured amplitude vs. distance curve (Instrument: Pico Plus AFM, Agilent Tec., Tempe Az, USA). (c) Simulated second harmonic amplitude vs. distance curve. (d) Experimental second harmonic amplitude vs. distance curve obtained using an external Lock-in amplifier (SR 830 DSP, Stanford Research Systems, Sunnyvale Cal., USA). (e) Frequency spectra (normalized by the driving frequency) obtained from simulation for $A_{sp}/A_0 = 0.9$. (f) Measured frequency spectra (normalized by the driving frequency, recorded using a NI PCI-6013 data acquisition device).

[15]. For the cantilever properties in [Eq. (1)–(3)], values obtained by fitting a Lorentzian to experimental tuning curves of the free cantilever were used. The so determined Q -factor, mass, and resonance frequency were 2.078, 353 ng, and 8.46 kHz, respectively. The tip radius was assumed to be 20 nm, and the other parameters were chosen from literature ([13,14]) for a silicon nitride tip

($k = 0.1$ N/m) and a mica surface interacting through water (Hamaker constant $H = 3.1 \times 10^{-21}$ J).

The simulated amplitude vs. distance curve is shown in Fig. 1(a) for a free amplitude of $A_0=4$ nm and a driving frequency f_d of 7.2 kHz. For comparison, Fig. 1(b) shows an experimental amplitude vs. distance curve obtained for the same A_0 and the same materials. At distances smaller

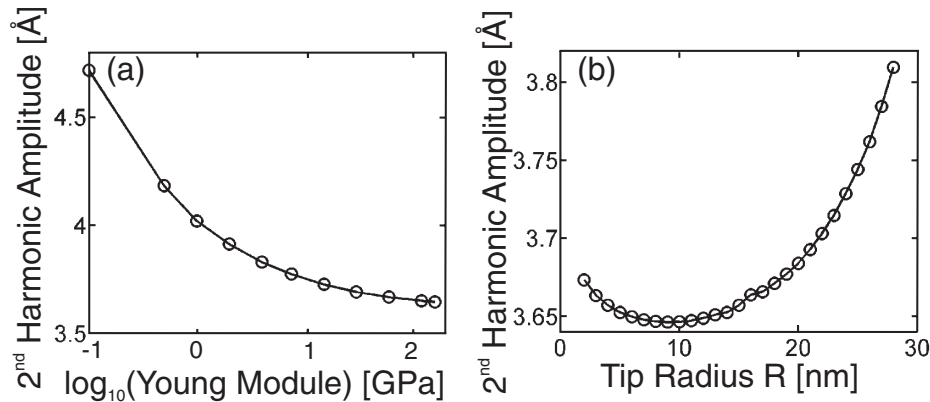


FIG. 2. Dependence of the second harmonic amplitude (A_2) on interaction parameters. (a) A_2 as a function of effective tip radius. (b) A_2 as a function of the samples Young module.

than A_0 , the tip senses the tip-sample interaction forces, which leads to the characteristic amplitude decrease. In this region, energy is transferred into higher harmonics (i.e., integer multiples) of the cantilever angular frequency. The contribution of the second harmonic, A_2 , is shown in Fig. 1(c) for the simulation and in Fig. 1(d) for the experiment. In both cases, a qualitatively similar initial and final decrease of A_2 along the tip-sample distance can be observed. Interestingly, the second harmonic amplitude was about 1 order of magnitude greater than the values reported from experiments performed in air [9]. The frequency spectra for a relative amplitude reduction $A_{sp}/A_0 = 0.9$ is shown in Figs. 1(e) and 1(f), revealing good accordance between simulation and experiment. From the experimental spectra, an estimate for the measurement noise of ~ 3 pm can be given. To show the sensitivity of A_2 for variations in the sample elasticity and the interaction area (in terms of different effective interaction radii), the Young module and the tip radius were varied in characteristic regimes, respectively, by assuming H to be constant. Figure 2 shows the dependence of the calculated second harmonic amplitude on the Young modulus of the sample [Fig. 2(a)] and on the effective tip radius [Fig. 2(b)] for $A_{sp}/A_0 = 0.9$. Since the experimentally observed noise (~ 3 pm) is rather small compared to the calculated dependencies of A_2 on these interaction parameters, the simulation suggests the use of the second harmonic amplitude for mapping the elastic and geometric properties of the tip-sample interaction.

To verify the potential of this method, second harmonic amplitude and topography images were simultaneously recorded ($A_0 \sim 10$ nm, $A_{sp}/A_0 = 0.85$, $f_d = 7.3$ kHz, $k = 0.1$ N/m, BPS buffer) on the surface of *S*-layer rSbpA-*strep*-tagII recrystallized on cleaned silicon [16]. The topography image [Fig. 3(a), left panel] reveals a lattice with p4 symmetry and a periodicity of ~ 14 nm, which is in agreement with the structure known from literature [16]. In addition to this, the second harmonic image [Fig. 3(a), right panel] shows detailed substructures within the unit cell of the *S*-layer. Even at areas where the topographical image is blurred due to the underlying roughness of the silicon surface, the second harmonic image clearly resolves the local properties of the protein lattice. Frequency spectra were recorded on two distinct positions of the sample, Fig. 3(a), showing the anharmonic contributions to the tip motion [Fig. 3(b)] at a hole (position 1) and at the position occupied by a protein (position 2) (note that the amplitude scale is logarithmic and the spectra are shifted with respect to the normalized driving frequency for better visibility). The corresponding second harmonic amplitude values [Fig. 3(a), inset] of 0.72 (position 1) and 0.78 nm (position 2) yielded a difference (60 pm) well above the noise level (~ 3 pm). In accordance with the simulations, different anharmonic contributions were observed in the whole frequency range reflecting the

underlying variation of the tip-sample interaction. The strong dependence of the second harmonic amplitude on elasticity differences [Fig. 2(a)] and interaction geometries [Fig. 2(b)] can be attributed to the significant amount of energy transferred from the driving frequency to its second harmonic, when nonlinear tip-sample interaction occur [9] in a highly over-damped system. The enhanced lateral resolution arising from this effect is demonstrated in Fig. 3(c). An average of 55 unit cells (left panel) of the

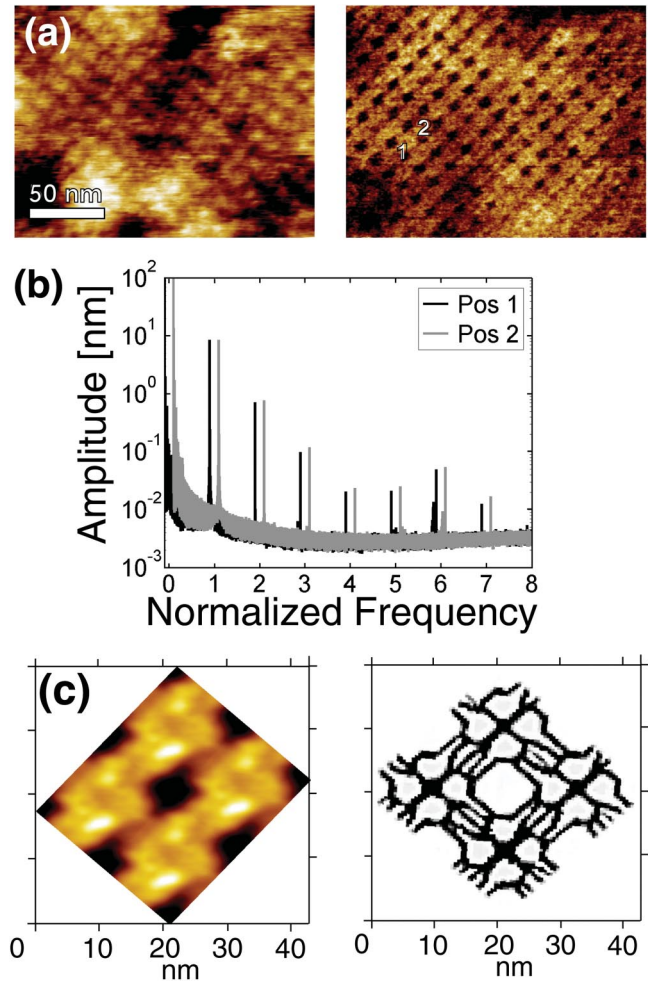


FIG. 3 (color). High resolution on a bacterial *S*-layer. Second harmonic images were recorded using an external Lock-in amplifier (SR 830 DSP, Stanford Research Systems, Sunnyvale Cal., USA). (a) Simultaneous recorded topography (left panel) and second harmonic image (right panel). Substructures within the unit cell can be clearly observed (resolution ~ 0.5 nm). Scansize: 210×175 nm²; color code: 0–0.9 nm, 0–0.5 V. (b) Frequency spectra recorded on positions 1 and 2 of (a). The spectral contributions reflect the different properties of the tip-protein (pos. 2) and tip-hole (pos. 1) interactions (note that spectra are shifted with respect to the normalized driving frequency for better visibility). Inset: Contribution of the second harmonic amplitude in linear representation. (c) Average of 55 unit cells (left panel) from a (right panel) and a sketch of the expected lattice structure (right panel) 16.

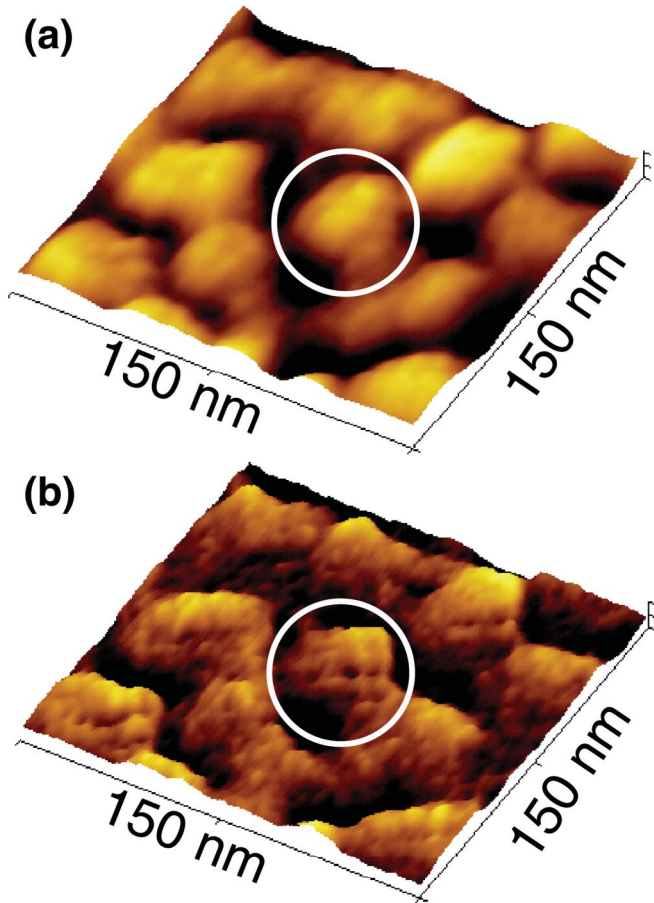


FIG. 4 (color). Measurements on human rhinovirus serotype 2 (HRV2). (a) Topography image of HRV2 layer on mica. (b) Simultaneously recorded second harmonic amplitude image clearly revealing substructures of the viral capsids (circle). Scansize: $350 \times 350 \text{ nm}^2$; color code: 0–13 nm, 0–0.35 V.

second harmonic image [Fig. 3(a), right panel] clearly reveals the structure known from literature [17], Fig. 3(c) right panel. Second harmonic amplitude images were also recorded ($A_0 \sim 15 \text{ nm}$, $A_{sp}/A_0 = 0.9$, $f_d = 7.9 \text{ kHz}$, $k = 0.1 \text{ N/m}$, Ni-Tris buffer) from human rhinovirus serotype 2 (HRV2) [18], electrostatically bonded to a clean mica surface [19]. A fairly dense layer of HRV2 (spherical shape, diameter $\sim 30 \text{ nm}$) can be observed in the topography image [Fig. 4(a)], whereas the second harmonic amplitude image reveals details of the capsid structure (circle) of the virus [Fig. 4(b)]. These substructures might reflect the protrusions on the surface of the viral capsid known from cryo-EM and x-ray imaging [18,20].

These examples demonstrate that mapping higher harmonics of the cantilever motion under highly over-damped conditions in liquids provides additional information on the sample properties, since the sensitivity of these higher harmonic amplitudes is strongly enhanced compared to the operation in air.

We thank Drs. Nicola Ilk and Uwe Sleytr for generously providing the rSbpA-*strep*-tagII and Dr. Dieter Blaas for providing the HRV2. This work was supported by the European Commission (FORCETOOL, No. NMP3-CT-2004-013684, NAS-SAP, No. NMP3-CT-2004-013532).

*Corresponding author: Institute for Biophysics, J. Kepler University of Linz Altenbergerstrasse 69, A-4040 Linz, Austria. Tel.: ++43-732-2468-9265, Fax: ++43-732-2468-9270
peter.hinterdorfer@jku.at

- [1] G. Binnig, C. F. Quate, and C. Gerber, *Phys. Rev. Lett.* **56**, 930 (1986).
- [2] W. Han, S. M. Lindsay, and T. Jing, *Appl. Phys. Lett.* **69**, 4111 (1996).
- [3] P. K. Hansma *et al.*, *Appl. Phys. Lett.* **64**, 1738 (1994).
- [4] C. A. J. Putman *et al.*, *Appl. Phys. Lett.* **64**, 2454 (1994).
- [5] S. H. Leuba *et al.*, *Proc. Natl. Acad. Sci. U.S.A.* **91**, 11621 (1994).
- [6] M. Stark *et al.*, *Biophys. J.* **80**, 3009 (2001).
- [7] J. Tamayo and R. Garcia, *Appl. Phys. Lett.* **71**, 2394 (1997).
- [8] J. Tamayo and R. García, *Appl. Phys. Lett.* **73**, 2926 (1998).
- [9] R. W. Stark and W. M. Heckl, *Rev. Sci. Instrum.* **74**, 5111 (2003).
- [10] R. Garcia and R. Perez, *Surf. Sci. Rep.* **47**, 197 (2002).
- [11] C. Rankl *et al.*, *Ultramicroscopy* **100**, 301 (2004).
- [12] O. Teschke, G. Ceotto, and E. F. de Souza, *Phys. Rev. E* **64**, 011605 (2001).
- [13] R. Garcia and A. San Paulo, *Phys. Rev. B* **60**, 4961 (1999).
- [14] J. N. Israelachvili, *Intermolecular and Surface Forces* (Academic Press, London, UK, 1992).
- [15] W. H. Press, S. A. Teukolsky, W. T. Vetterling, and B. P. Flannery, *Numerical Recipes in C* (Cambridge University Press, Cambridge, UK, 1988).
- [16] C. Vollenkle *et al.*, *Appl. Environ. Microbiol.* **70**, 1514 (2004).
- [17] U. B. Sleytr *et al.*, *Prog. Surf. Sci.* **68**, 231 (2001).
- [18] N. Verdagner, D. Blaas, and I. Fita, *J. Mol. Biol.* **300**, 1179 (2000).
- [19] F. Kienberger *et al.*, *Structure* **13**, 1247 (2005).
- [20] E. A. Hewat and D. Blaas, *EMBO J.* **15**, 1515 (1996).